Quantum computing of quantum chaos in the kicked rotator model

B. Lévi, B. Georgeot, and D. L. Shepelyansky
Laboratoire de Physique Quantique, UMR 5626 du CNRS, Université Paul Sabatier, F-31062 Toulouse Cedex 4, France
(Received 21 October 2002; revised manuscript received 6 February 2003; published 25 April 2003)

We investigate a quantum algorithm that simulates efficiently the quantum kicked rotator model, a system that displays rich physical properties and enables to study problems of quantum chaos, atomic physics, and localization of electrons in solids. The effects of errors in gate operations are tested on this algorithm in numerical simulations with up to 20 qubits. In this way various physical quantities are investigated. Some of them, such as second moment of probability distribution and tunneling transitions through invariant curves, are shown to be particularly sensitive to errors. However, investigations of the fidelity and the Wigner and Husimi distributions show that these physical quantities are robust in presence of imperfections. This implies that the algorithm can simulate the dynamics of quantum chaos in presence of a moderate amount of noise.

DOI: 10.1103/PhysRevE.67.046220 PACS number(s): 05.45.Mt, 03.67.Lx, 72.15.Rn

I. INTRODUCTION

It is only recently that it was realized that quantum mechanics can be used to process information in fundamentally new ways. In particular, Feynman [1] emphasized that the massive parallelism due to the superposition principle may allow to simulate efficiently some problems intractable on classical computers, the most obvious being many-body quantum systems. Since that time, a model of quantum computer has been set up, viewed as an ensemble of *n qubits*, i.e., two-level systems, with a Hilbert space of dimension 2^n (see reviews [2–4]). Computation is performed through unitary transformations applied to the quantum wave functions of this many-body system. In fact, it has been shown that any unitary transformation on this 2^n-dimensional space can be written in terms of a set of universal gates, for example, one- and two-qubit transformations. Also, important quantum algorithms have been developed, such as Shor's algorithm for factoring large numbers [5], which is exponentially faster than any known classical method, and Grover's algorithm to search a database [6], where the gain is polynomial.

Motivated by these developments, many experimental implementations for actual realization of such a quantum computer were proposed (see Ref. [4] and references therein). Recent results include, for example, the NMR implementation of factorization algorithm with seven qubits made from nuclear spins in a molecule [7] and the simulation of the quantum baker map [8]. Thus, small quantum computers with a few qubits are already available experimentally, and systems of larger size can be envisioned at relatively short term.

Still, algorithms such as that of Shor require large number of qubits and the use of many gates. It is, therefore, important to develop algorithms that need a smaller number of qubits and gates and still can yield interesting quantities. In particular, algorithms enabling to simulate quantum mechanical systems, as originally envisioned by Feynman, can be implemented relatively easily and solve problems inaccessible to classical computers with less expense in number of qubits and gates. Several such algorithms have been developed for various systems, including many-body Hamiltonians [9] or spin lattices [10]. An especially interesting class of systems corresponds to chaotic quantum maps. Such systems can have a very complex dynamics while their Hamiltonians keep a relatively simple form. Algorithms for fast simulation on a quantum computer were built for the quantum baker map [11], the kicked rotator [12], and the sawtooth map [13]. We note that recently the quantum baker map was implemented on a NMR quantum computer [8]. The kicked rotator is an especially rich and generic system, which has been a cornerstone for the study of quantum chaos [14]. In the classical limit it reduces to the Chirikov standard map, which has been also extensively studied in the field of classical chaos [15]. Implementation of this model can be done on a small quantum computer with a few tens of qubits, and classical supercomputers will be outperformed with a few hundreds of qubits. Still, real quantum computers will not be free of imperfections and errors, and this will affect the results of the computation. It is, therefore, important to understand the effects of different sources of errors on the results of such an algorithm. For example, first numerical simulations of the quantum computation of this model [16] have shown that errors affect in a different way the various physical quantities characterizing the model, and that for some of them the effect of errors can be exponentially strong.

In this paper, after presenting in more detail the physics of the kicked rotator, we study the effects of errors on several physical quantities. We focus on random unitary errors, which may arise when imperfect gates are applied, and study first how global quantities such as second moment or fidelity are affected by errors. Our results confirm and extend those obtained in Ref. [16] showing a marked contrast in the behavior of these two quantities in presence of errors. We also investigate how well the whole wave function is reproduced by an imperfect quantum computer. A particularly interesting way to display wave functions is to express them through phase-space distributions, such as the Wigner and Husimi functions. These distributions display the same information as the wave functions, but in a form which allows direct comparisons between classical and quantum dynamics, a property especially interesting to probe the classical limit of quantum mechanics. They have been extensively used in many fields, and recently a method has been devised [17] to

measure such distribution for quantum simulations on quantum computers. The effects of errors on the Wigner and Husimi functions will be investigated in details, showing how imperfections affect the different parts of phase space, and discussing how information can be retrieved through quantum measurement. A separate section is focused on how a localized distribution may escape from an island of integrability, showing an especially large effect of quantum errors on a quantity that is directly relevant to quantum tunneling.

II. THE KICKED ROTATOR

The classical kicked rotator is described by the Chirikov standard map [14,15]:

$$\overline{n} = n + k \sin\theta, \quad \overline{\theta} = \theta + T\overline{n}, \tag{1}$$

where (n,θ) is the pair of conjugated momentum (action) and angle variables, and the bars denote the resulting variables after one iteration of the map. It describes a free angle rotation and a kick in momentum. This area-preserving map has been extensively studied during the past decades and has been applied to problems such as particle confinement in magnetic traps, beam dynamics in accelerators, comet trajectories, and many others [15].

The dynamics of this map takes place on a cylinder (periodicity in θ) and is controlled by a single parameter $K=kT$. For $K=0$ the system is integrable and all trajectories lie on one-dimensional tori (lines $n=$constant). For $K>0$, the system undergoes a transition to chaos, which follows the Kolmogorov-Arnold-Moser (KAM) theorem. Periodic orbits corresponding to rational frequencies are transformed into chains of integrable islands mixed with chaotic region. On the contrary, tori with irrational frequencies are deformed but survive, forming invariant curves that separate zones in phase space. As K is increased, these surviving tori become Cantor sets (cantori) and disappear. The most robust torus corresponds to the golden number $(1+\sqrt{5})/2$, and disappears for $K=K_g\approx 0.9716\ldots$. Thus, for $K>K_g$ global chaos sets in, with appearance of an extended chaotic region in phase space and with dynamics characterized by a positive Kolmogorov-Sinai entropy $h\approx\ln(K/2)>0$ (for $K\geqslant 6$). In this régime, a typical trajectory shows diffusive growth of momentum, which statistically can be described by the Fokker-Planck equation, with diffusion rate $D=n^2/t\approx k^2/2$, where t is measured in number of iterations (kicks) [14,15]. For lower values of K, the phase space displays a complex hierarchical structure with integrable islands surrounded by chaotic zones at smaller and smaller scales.

Map (1) is periodic in n with period $2\pi/T$, so the phase-space structures repeat themselves on each cell of size $2\pi/T$. Such a cell is shown in Fig. 1 for $K=K_g$, displaying the complex hierarchical structures that appear in the phase space.

The quantization of Eq. (1) yields a Hamiltonian, which after integration over one period gives a unitary evolution operator acting on wave function ψ:

$$\overline{\psi} = \hat{U}\psi = e^{-ik\cos\hat{\theta}} e^{-iT\hat{n}^2/2}\psi, \tag{2}$$

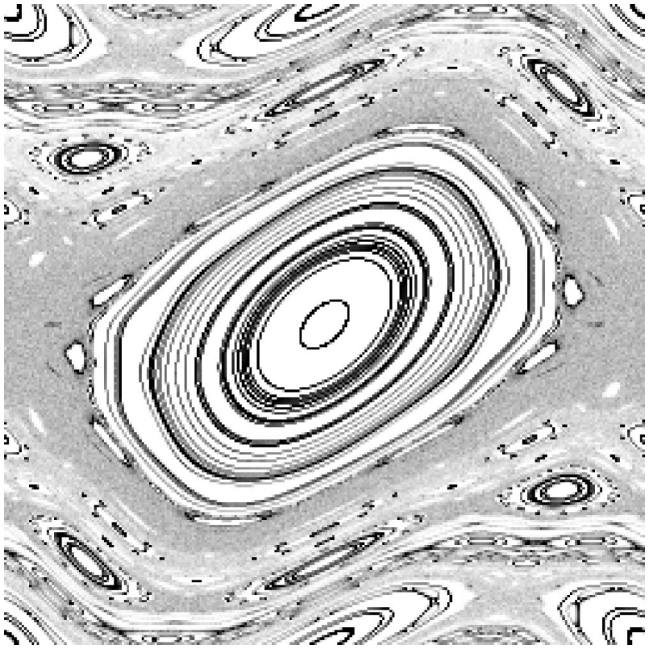

FIG. 1. Plot of the classical phase space at $K=K_g=0.9716\ldots$ [$t=10^4$ iterations of Eq. (1) for 200 points].

where $\hat{n}=-i\partial/\partial\theta$, $\hbar=1$, and $\psi(\theta+2\pi)=\psi(\theta)$. The quantum dynamics depends on two parameters k and T (instead of the single parameter $K=kT$ for the classical one). The classical limit corresponds to $k\to\infty$, $T\to 0$ while keeping $K=kT=$constant [14,18,19]. In a sense, T plays the role of an effective $\hbar$.

Depending on the values of theses parameters, the system follows different régimes, from regularity to quantum chaos. Due to this variety of behaviors, the quantum kicked rotator has been intensively studied (see Refs. [14,18,19] and references therein). Indeed, most of the phenomena characteristic of quantum chaos are present, such as quantum ergodicity, random matrix theory statistics, chaos assisted tunneling, and others. In particular, for $K>K_g$, the phenomenon of dynamical localization appears. Although in this régime a typical classical trajectory diffuses in momentum, eigenstates $\chi_m(n)$ of operator $\hat{U}$ in momentum space are exponentially localized for typical values of k and T. Their envelopes obey the law $\chi_m(n)\sim\exp(-|n-m|/l)/\sqrt{l}$, where m marks the center of the eigenstate and l is the localization length. For $k\gg K\gg 1$ this length is determined by the classical diffusion rate $l=D/2\approx k^2/4$ [18]. This phenomenon has close relationship with the Anderson localization of electrons in disordered solids [20], and investigation of the kicked rotator gives information on this important solid-state problem still under intensive investigation nowadays. The quantum kicked rotator describes also the properties of microwave ionization of the Rydberg atoms [21]. It has been realized experimentally with cold atoms, and the effects of dynamical localization, external noise, and decoherence have been studied experimentally [22].

For numerical studies of quantum evolution (2) it is convenient to choose the case of quantum resonance with $T/(4\pi)=M/N$, where M,N are integers [19]. In this way

the quantum dynamics takes place on a torus with N levels. For $l \gg N$ the eigenstates of evolution operator become ergodic and the level spacing statistics is described by the random matrix theory [19].

The algorithm for the quantum simulation of the kicked rotator was presented in Ref. [12]. Evolution (2) consists of the product of two unitary operators that are diagonal in the angle and momentum bases, respectively. The most efficient classical algorithm available consists in changing back and the forth between the angle and the momentum representation by the fast Fourier transforms (FFT). The operator that is diagonal in the basis is then implemented by direct multiplication of the coefficients of the wave function. In total, one iteration of Eq. (2) on a Hilbert space of dimension $N = 2^{n_q}$ requires $O(N \log N)$ classical operations, the limiting steps being the FFT. The quantum algorithm follows the classical one, and speeds up all parts of it to obtain exponential increase of computation rate. First, an initial distribution is built, in a polynomial number of operations (in n_q). Various initial wave functions can be built in this way. In the following, we will use as initial state $|\Psi_0\rangle$ a wave function localized at a precise value of momentum n, which can be built in n_q single-qubit rotations starting from the ground state. The general state of the system can be written as $\Sigma_{n=0}^{N-1} a_n |n\rangle$, where a_n are the amplitudes of the wave function on the $|n\rangle$ basis state. Then the first unitary operator is applied. In the n representation it is diagonal and can be written as $\exp(-iTn^2/2)$. This operator can be implemented efficiently by using the binary decomposition of n: if $n = \Sigma_{j=0}^{n_q-1} \alpha_j 2^j$, then $n^2 = \Sigma_{j_1,j_2} \alpha_{j_1} \alpha_{j_2} 2^{j_1+j_2}$. Therefore, $\exp(-iTn^2/2) = \Pi_{j_1,j_2} \exp(-iT\alpha_{j_1}\alpha_{j_2} 2^{j_1+j_2-1})$ with $\alpha_{j_{1,2}} = 0$ or 1. Thus, one needs to implement the two-qubit gate applied to each qubit pair (j_1, j_2) that keeps the states $|00\rangle, |01\rangle, |10\rangle$ unchanged, while $|11\rangle$ is transformed to $\exp(-iT2^{j_1+j_2-1})|11\rangle$. $O(n_q^2)$ applications of this gate are sufficient to simulate $\exp(-iTn^2/2)$.

Then a quantum Fourier transform (QFT) (see, e.g., Ref. [2]) is performed to shift from n to θ representation, yielding $\Sigma_{i=0}^{N-1} b_i |\theta_i\rangle$. This transformation needs only $O(n_q^2)$ one- and two-qubit gates, and yields the wave function in θ representation. In this representation, the second operator $\exp(-ik\cos\hat{\theta})$ is diagonal. Direct (sequential) multiplication by $\exp(-ik\cos\theta_i)$ for each θ_i will require exponentially many operations, so a parallel way to apply this operator has to be devised. In Ref. [12], it was proposed to use supplementary registers in which the values of $\cos(\theta_i)$ will be computed in parallel. The procedure transforms $\Sigma_{i=0}^{N-1} b_i |\theta_i\rangle |0\rangle$ into $\Sigma_{i=0}^{N-1} b_i |\theta_i\rangle |\cos\theta_i\rangle$, with $\cos(\theta_i)$ computed up to a fixed precision using a recursive method based on Moivre's formula [12]. This is actually the slowest step of the algorithm, requiring $O(n_q^3)$ elementary operations. From the state $\Sigma_{i=0}^{N-1} b_i |\theta_i\rangle |\cos\theta_i\rangle$, it is easy by using n_q one-qubit operations to build the state $\Sigma_{i=0}^{N-1} b_i \exp(-ik\cos\theta_i) |\theta_i\rangle |\cos\theta_i\rangle$. Then the cosines in the last register are reversibly erased by running backward the sequence of gates that constructed them, and one ends up with the state $\Sigma_{i=0}^{N-1} b_i \exp(-ik\cos\theta_i) |\theta_i\rangle |0\rangle$, which is the result of the action of the unitary operator $\exp(-ik\cos\hat{\theta})$. Another QFT [requiring $O(n_q^2)$ operations] takes the wave function back to the n representation.

Increasing n_q, which exponentially increases the dimension of the Hilbert space available, enables to probe various physical limits in the system. If $K = kT$ is kept constant, the classical mechanics remains the same. If T is kept constant, the effective $\hbar$ is fixed, and increasing n_q will increase exponentially the size of the phase space of the system (number of cells). In contrast, if $T = 2\pi/N$, with $N = 2^{n_q}$, the size of the phase space remains the same, all N momentum states correspond to the same cell of size $2\pi/T$. In this case, increasing n_q increases the number of quantum levels corresponding to the same classical structure, and is equivalent to decreasing $\hbar$ toward the classical limit.

The whole quantum algorithm described above requires $O(n_q^3)$ gate operations to perform one iteration of quantum map (2), exponentially less than the classical algorithm. Still, a physical quantum computer will not be an ideal perfect machine, and there will be imperfections, which may hamper the computation. In the following sections, we will investigate the effects of noise and imperfections on the physical quantities that are simulated, and estimate the accuracy of the quantum computation of quantum map (2). The numerical simulation of many qubits is very resource consuming on a classical computer. Due to that we took in all numerical computations the action of $\exp(-ik\cos\hat{\theta})$ as exact, and performed by direct multiplication in θ representation all other operations being made with errors. We think that this approximation does not alter the qualitative features of the results, although the number of quantum gates is reduced from $O(n_q^3)$ to $O(n_q^2)$. Also in this approximation all supplementary registers required for the computation of $|\cos\theta_i\rangle$ are eliminated and the quantum evolution on $N = 2^{n_q}$ levels is performed with only n_q qubits.

III. GLOBAL QUANTITIES

We first study the effects of imperfections and errors for the global quantities of the system.

To model these imperfections, we introduce a random unitary error during the operation of elementary quantum gates. These errors are present for each gate performing the quantum Fourier transform and the action of the unitary operator $e^{-iT\hat{n}^2/2}$. Two elementary gates are used: the single-qubit Hadamard gates $H = \mathrm{diag}(1,1,1,-1)$ and the two-qubit gate $B = \mathrm{diag}(1,1,1,\exp(i\alpha))$, where α is a phase. Transformation H can be written as $H = \vec{u}_0 \cdot \vec{\sigma}$, where $\vec{u}_0 = (1/\sqrt{2}, 0, 1/\sqrt{2})$ and $\vec{\sigma} = (\sigma_x, \sigma_y, \sigma_z)$. It is replaced by an imperfect gate $H' = \vec{u} \cdot \vec{\sigma}$, where $\vec{u}$ is a unit vector with a random angle β from $\vec{u}_0$. In a similar way, each B is replaced by $B' = \mathrm{diag}(1,1,1,\exp(i\alpha + i\gamma))$, where γ is again a random angle. At a given strength $\epsilon > 0$ of noise, each gate is implemented with a β or γ randomly selected from a uniform distribution such that $|\beta| < \pi\epsilon$ or $|\gamma| < \pi\epsilon$ [23]. As explained in Sec. II, we made the approximation of taking the action of $\exp(-ik\cos\hat{\theta})$ as exact, all other operations being made with

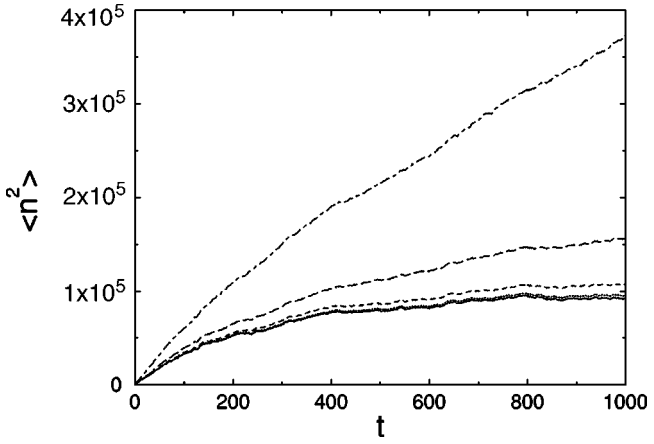

FIG. 2. Dependence of the second moment $\langle n^2\rangle=\langle(n-n_0)^2\rangle$ of the probability distribution on time t for $T=0.5$ and $K=15$. Data are shown from top to bottom for $n_q=16,15,14,13$ and $\epsilon=10^{-4}$ (four curves). The lowest fifth full curve is for $\epsilon=0$, $n_q=14$. The initial state is $|\Psi_0\rangle=|n_0\rangle$, with $n_0=N/2$.

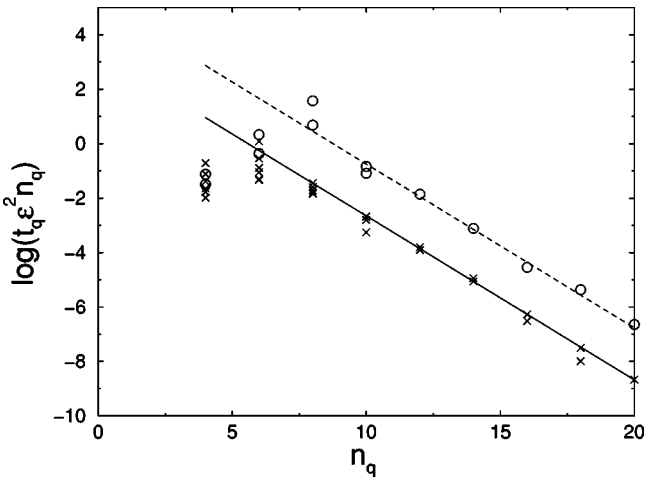

FIG. 3. Dependence of the rescaled time scale t_q on the number of qubits n_q for $10^{-6}<\epsilon<0.03$, $T=0.5$, $K=5$ ($\times$), and $K=15$ ($\bigcirc$). The initial state is $|\Psi_0\rangle=|n_0\rangle$ with $n_0=N/2$. Data are averaged over 10 to 1000 realizations of noise. Full and dashed lines correspond to the theoretical formula (3) with $C_q=0.23$. The logarithm is decimal.

errors. The use of n_q qubits gives a Hilbert space for wave functions of the kicked rotator on N levels, with $N=2^{n_q}$, i.e., values of momentum range from $n=1$ to $n=N$. In all numerical computations, initial state $|\Psi_0\rangle$ was chosen as localized on a precise value of the momentum n_0, i.e., $|\Psi_0\rangle=|n_0\rangle$, with $n_0=1$ (lowest value of momentum) or $n_0=N/2$. The rotation is computed as $\exp[-iT(n-\overline{n})^2/2]$ with $\overline{n}=N/2$.

Depending on the choice of parameters in Eq. (2), increasing the number of qubits n_q will increase the number of values of momentum in each phase-space cell of size $\Delta n=2\pi/T$, or increase the number of cells, or both. In Ref. [16], it was shown that if T is constant while n_q increases, errors in the QFT may lead to an *exponential* growth of errors with n_q for the second moment $\langle n^2\rangle$ of the probability distribution. In this case, the size of phase space grows exponentially with n_q, but K and effective $\hbar$ are kept fixed. Due to quantum localization, exact wave functions cannot spread beyond a region of size given by the localization length, which remains fixed when n_q increases. Therefore for all values of n_q, the second moment of a distribution initially located at $n_0=N/2$ will saturate with time at a value independent of n_q (full line in Fig. 2) if Eq. (2) is exactly simulated. On the contrary, errors in the QFT lead to small transfer of probabilities to the regions of phase space that are exponentially far away from where the exact wave function is localized. This induces the exponential increase of the second moment with n_q. We confirm here this effect in Fig. 2 for different parameters with more complete set of errors used in this paper, and with simulations up to larger number of qubits.

To be more quantitative, Fig. 3 shows the time scale t_q on which the presence of errors leads to a doubling of the value of the second moment $\langle n^2\rangle$ as a function of n_q and error strength ϵ. In Ref. [16] the formula

$$t_q\approx C_q k^4/(\epsilon^2 n_q 2^{2n_q}) \tag{3}$$

was proposed and checked numerically with up to 13 qubits. It stems from the fact that each imperfect gate operation transfers on average a probability of ϵ^2 equally divided among n_q spurious peaks located at integer powers of 2. Thus, due to imperfections $\langle n^2\rangle\sim n_q\epsilon^2 2^{2n_q}t$ (each time step involves $\sim n_q^2$ gate operations), whereas for the exact wave function $\langle n^2\rangle\approx D^2\approx 4l^2\approx k^4/4$. Both expressions become comparable at time t_q given by Eq. (3). Figure 3 confirms this formula by extensive numerical computations, with up to 20 qubits, and for two different values of K. This enables to get the numerical constant $C_q\approx 0.23$.

Although time scale t_q drops exponentially with n_q, there are other observables that show only polynomial sensitivity to errors. A standard quantity used to characterize the global influence of errors is the fidelity defined by the projection of the wave function with errors $\psi_\epsilon(t)$ on the perfect one $\psi_0(t)$: $f(t)=|\langle\psi_\epsilon(t)|\psi_0(t)\rangle|^2$. The dependence of this fidelity on time in presence of errors is shown in Fig. 4, showing that it slowly decreases with t and amplitude of noise ϵ. One can define a time scale t_f such that $f(t_f)=0.5$. Figure 5 presents the variation of t_f with system parameters in two different régimes. It shows that the relation

$$t_f\approx C_f/(\epsilon^2 n_q^2) \tag{4}$$

holds with the numerical constant $C_f\approx 0.35$. Figures 4 and 5 are consistent with a fidelity decay $f(t)\sim\exp(-\Gamma t)$ where $\Gamma\sim\epsilon^2 n_q^2$.

Relation (4) can be understood from the following physical considerations. Each imperfect unitary gate is rotated by a random angle of order ϵ from the exact one. Therefore, a probability of order ϵ^2 is transferred from the exact state at each gate operation. Each time step of map (2) takes $O(n_q^2)$ operations, in the approximation that we have taken where the building of the cosines is supposed exact. This implies that t_f, which is in units of time steps of Eq. (2), should vary

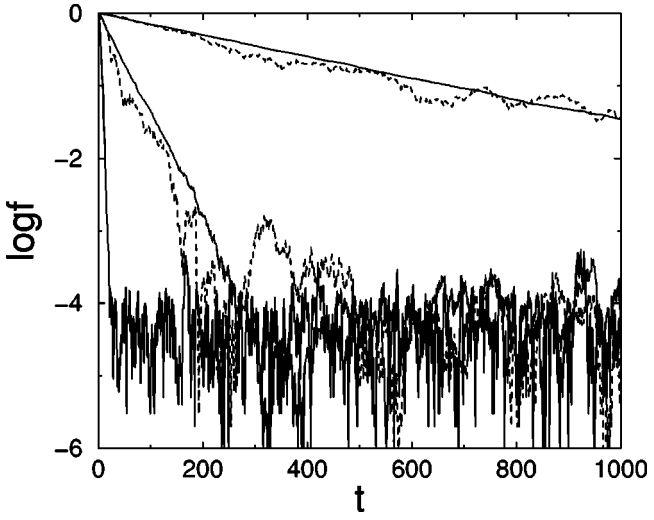

FIG. 4. Evolution of fidelity f with time t. Full curves are for $K=1.3$, $T=2\pi/N$ ($N=2^{n_q}$), $n_q=14$, and from top to bottom $\epsilon=3\times10^{-3}$, $\epsilon=10^{-2}$, $\epsilon=0.03$. The initial state is $|\Psi_0\rangle=|n_0\rangle$ with $n_0=1$. Dashed curves are for $T=0.5$, $K=5$, and $n_q=14$, and from top to bottom $\epsilon=3\times10^{-3}$, $\epsilon=10^{-2}$. The initial state is $|\Psi_0\rangle=|n_0\rangle$ with $n_0=N/2$. The logarithm is decimal.

as $1/(\epsilon^2 n_q^2)$. We expect that if the full algorithm was implemented, with the cosines computed following the procedure explained in Sec. II, a time step of Eq. (2) should take $O(n_q^3)$ operations, and accordingly t_f should vary as $1/(\epsilon^2 n_q^3)$.

The data shown in this section exemplify the sharp contrast in the behavior of the different observables in presence of errors. The fidelity shows only a polynomial decrease with respect to both ϵ and n_q, whereas the second moment of the wave function grows exponentially with n_q, but polynomially with ϵ. The resolution of this apparent paradox is related to the fact that the second moment is sensitive to the *size* of the Hilbert space, which grows exponentially with n_q. Small spurious peaks due to imperfections do not spoil the fidelity, but strongly modify the variance $\langle n^2\rangle$ if they appear very far away from the exact location of the wave function [24].

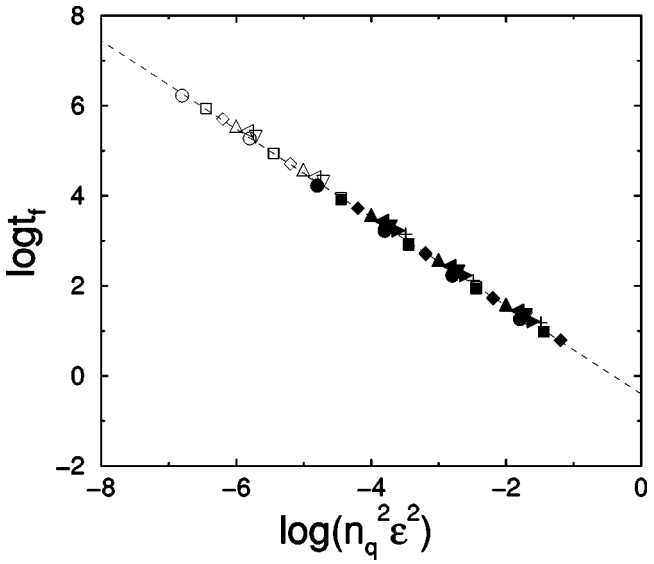

FIG. 5. Dependence of the time scale t_f on system parameters for $n_q=4$ (○), 6 (□), 8 (◇), 10 (△), 12 (◁), 14 (▽), 16 (▷), 18 (+). Here $K=1.3$, $T=2\pi/N$ ($N=2^{n_q}$) (open symbols) or $K=5$, $T=0.5$ (full symbols). The dashed line is the theoretical formula (4) with $C_f=0.35$. The initial state is $|\Psi_0\rangle=|n_0\rangle$, with $n_0=1$ ($K=1.3$) or $n_0=N/2$ ($K=5$). Data are averaged over 10 to 100 realizations of noise. Data for $T=0.5$ and $K=15$ are nearly indistinguishable from $T=0.5$, $K=5$ (not shown). Logarithms are decimal.

IV. WIGNER AND HUSIMI DISTRIBUTIONS

In the preceding section we focused mainly on the case where T (effective $\hbar$) is fixed but the phase-space size grows exponentially with n_q. In contrast, at $T=2\pi/N$ and $N=2^{n_q}$ the system size in classical momentum (number of $2\pi/T$ cells in n) remains fixed when n_q increases. In this way the effective $\hbar$ drops exponentially with n_q and going to larger number of qubits means approaching the classical limit (exponentially fast). Smaller and smaller details of the classical structure will be visible in the quantum wave functions. In this régime, data presented in Figs. 4 and 5 have already shown that the fidelity follows law (4) as in the case $T=$ constant. However, the fidelity characterizes in one number the accuracy of the whole wave function, and does not tell how well the local properties are reproduced. To study the local properties of wave functions, one can express it in θ or n representation. However, a very useful representation corresponds to phase-space distributions, such as the Wigner or Husimi distributions. They are especially used in the field of quantum chaos, since such representations permit a direct comparison with classical Hamiltonian mechanics, which takes place in phase space. They also enable to probe the classical/quantum border when $\hbar$ is decreased compare to other parameters of the system. Plotting such quantities in presence of errors allows to probe how local properties of the wave functions are sensitive to imperfections in the quantum algorithm.

An additional motivation to study such phase-space representations stems from the fact that recently an algorithm was proposed [17] that enables to compute the Wigner function on a chosen point in phase space by the use of an ancilla qubit.

For a continuous system with two conjugate variables p and q the Wigner transform [25] of a wave function ψ is defined by

$$W(p,q)=\int \frac{e^{-(i/\hbar)pq'}}{\sqrt{2\pi\hbar}}\psi\left(q+\frac{q'}{2}\right)^*\psi\left(q-\frac{q'}{2}\right)dq'. \quad (5)$$

In a discrete system with N-dimensional Hilbert space, one is led to define the Wigner function on a lattice of $2N\times 2N$ points (see, e.g., Ref. [26]). In the case of the kicked rotator, the formula becomes

$$W(\theta,n)=\sum_{m=0}^{N-1}\frac{e^{-(2i\pi/N)n(m-\Theta/2)}}{2N}\psi(\Theta-m)^*\psi(m), \quad (6)$$

with $\Theta = N\theta/2\pi$. The Wigner function is always real, but contrary to classical Liouville phase-space distributions it can take negative values. It verifies $\Sigma_i W(\theta_i, n) = |\psi(n)|^2$ and $\Sigma_i W(\theta, n_i) = |\psi(\theta)|^2$.

The Wigner transform has the drawback of being negative or positive. Nevertheless, coarse graining this function over cells of size $\hbar$ gives non-negative values. Such a procedure gives the *Husimi distribution* (see, e.g., Ref. [27]) that corresponds to a Gaussian smoothing of the Wigner function. In the case of the kicked rotator, the Husimi distribution can be computed through

$$h(\theta, n) = \sum_{m=n-N/2}^{n+N/2} \left(\frac{T}{\pi}\right)^{1/4} \frac{\psi(m)}{\sqrt{N}} e^{-(T/2)(m-n)^2} e^{im\theta}, \quad (7)$$

where the Gaussian for simplicity is truncated for values larger than $N/2$, and $\psi(m)$ is the wave function in momentum representation. The Husimi distribution is always non-negative, and allows a direct comparison between classical Liouville density distributions and quantum wave functions.

The Wigner and Husimi distributions of wave functions of the quantum kicked rotator simulated on a quantum computer are shown in Fig. 6 for different level of errors. Both functions have similar patterns, although as expected the Wigner function displays interference structures absent in the Husimi distribution. In the regime of parameters studied, classical invariant curves are still present in phase space and prevent the exact wave function to enter the large elliptical island in the middle. In the presence of moderate level of noise, main structures are still present and distinguishable.

Figure 7 confirms this result, showing the Husimi distribution for larger number of qubits, together with the classical phase-space distribution. The Husimi distributions in phase-space show features mimicking the classical phase space distributions, in accordance with the correspondence principle. Figure 7 (left) shows that when n_q is changed, finer and finer details of the classical structures are visible in the exact quantum wave function, in accordance with the fact that increasing n_q amounts to reduce $\hbar$ and approach the classical limit. The same figure shows that the wave function is spread over a larger domain of phase space as n_q increases. This can be explained by the following effect. In this mixed régime between integrability and strong chaos at $K = 1.3$, the invariant classical curves that prevent any transport are no longer present since the last one is destroyed at $K = K_g = 0.97\ldots$. But *cantori* are present, which are remnants of the disappeared invariant curves. They have a fractal structure, and a wave packet can cross them only if the holes are large enough. These holes scale as $(K - K_g)^3$ and become comparable with the minimal area scale of the Husimi distribution determined by the effective $\hbar$ given by T. Hence, for $K - K_g \ll 1$, the wave function is prevented to cross the cantorus for $(K - K_g)^3 < T$. Due to that quantum interference prevents the transport via cantori [14,18,28].

The quantum Husimi distributions shown in Figs. 6 and 7 display structures of increasing complexity with larger n_q. Still, with moderate level of noise, the quantum computer is able to reproduce the exact distributions with reasonable accuracy. For larger errors in gate operations, significant probability is present at wrong phase-space locations, and phase-space structures become blurred. The comparison with the effect of classical noise visible in Fig. 7 shows that in this case the quantum errors enable the wave function to enter classically forbidden zones much faster, a fact that will be analyzed in more details in the following section.

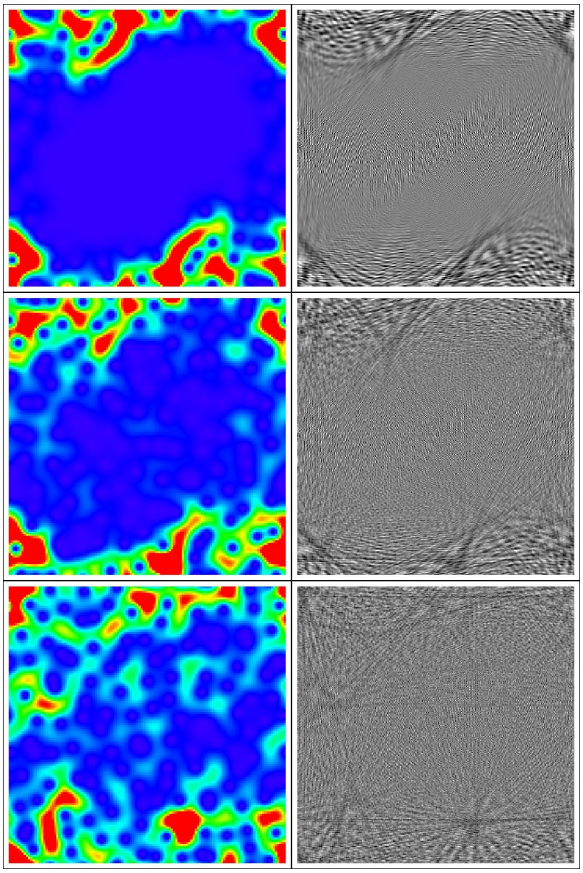

FIG. 6. (Color on line) Plot of Husimi (left) and Wigner (right) distributions at $t = 10^3$ for $K = 1.3 > K_g$, $T = 2\pi/N$, $N = 2^{n_q}$, and $n_q = 7$. The initial state is $|\Psi_0\rangle = |n_0\rangle$, with $n_0 = 1$. Top, $\epsilon = 0$; middle, $\epsilon = 0.002$; bottom, $\epsilon = 0.004$. Left: color (grayness) represents the intensity level from blue (white) (minimal) to red (black) (maximal). Right: grayness represents the amplitude of the Wigner function, from white (minimal negative value) to black (maximal positive value).

It is interesting to evaluate the effects of noise and imperfections not only on the broad features of the full Wigner function, but also on individual values. In Figs. 8 and 9, the behavior of individual values of the Wigner function in presence of noise in the gates is investigated. Figure 8 shows that the *relative* error (i.e., the error $\langle |W - W_\epsilon| \rangle$ divided by the average individual value of the exact Wigner function $\langle |W| \rangle$) increases slowly with the growth of t and ϵ even in the chaotic zone. Similar results can be observed in the integrable zone and in the localized régime (data not shown). In a more quantitative way, Fig. 9 shows the behavior of time scale t_W when the error on the Wigner function become comparable to its mean value in the régime chosen $[\langle |W(t_W) - W_\epsilon(t_W)| \rangle = \langle |W| \rangle / 2]$. In all three cases considered, one obtains

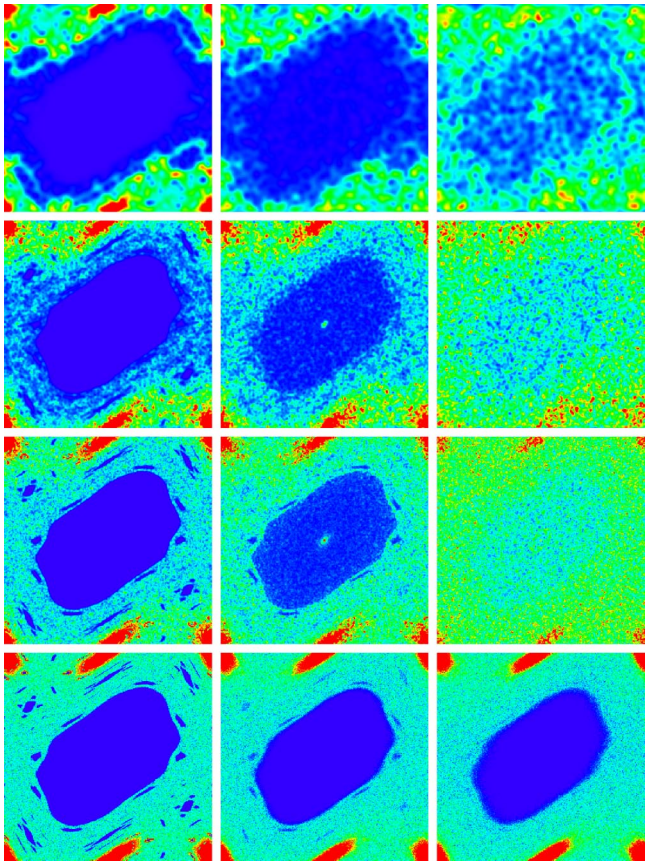

FIG. 7. (Color on line) First three rows: the Husimi distribution at $t=10^3$ for $K=1.3>K_g$ and $T=2\pi/N$, $N=2^{n_q}$; from top to bottom: $n_q=9$, $n_q=12$, $n_q=14$; quantum noise $\epsilon=0$ (left), $\epsilon=0.002$ (center), $\epsilon=0.004$ (right). Bottom row: the classical phase-space distribution at $t=10^3$ with classical noise $\epsilon=0$ (left), $\epsilon=0.002$ (center), $\epsilon=0.004$ (right). For clarity, the distributions are averaged over ten iterations around $t=10^3$. The initial quantum or classical state is $n_0=1$. Color (grayness) represents the intensity level from blue (white) (minimal) to red (black) (maximal).

$$t_W \approx C_W/(n_q^{\alpha}\epsilon^2), \tag{8}$$

with $\alpha=1$ or $\alpha=1.5$. Thus, individual values of the Wigner function in the kicked rotator model are robust quantities with respect to noise, even in the chaotic régime. These results are interesting also in view of the recent discussion on the effects of decoherence on the Wigner functions [29]. Our results clearly show that in the framework of quantum computation, the errors on the Wigner function are polynomial and not exponential.

As noted previously, a recent algorithm [17] enables to measure the value of the Wigner function of a system of density matrix ρ on a selected point in phase space, with the help of an ancilla qubit a. First, H (Hadamard gate) is applied on a, followed by a controlled-U operation (U is applied to the system to be measured depending on the state of a) and again H is applied on a. Then the expectation value of a is $\langle\sigma^z\rangle=\mathrm{Re}[\mathrm{Tr}(U\rho)]$. The use of a particular operator U, which can be implemented efficiently [17], enables to get $W(p,q)=\langle\sigma^z\rangle/2N$ (where $N=2^{n_q}$).

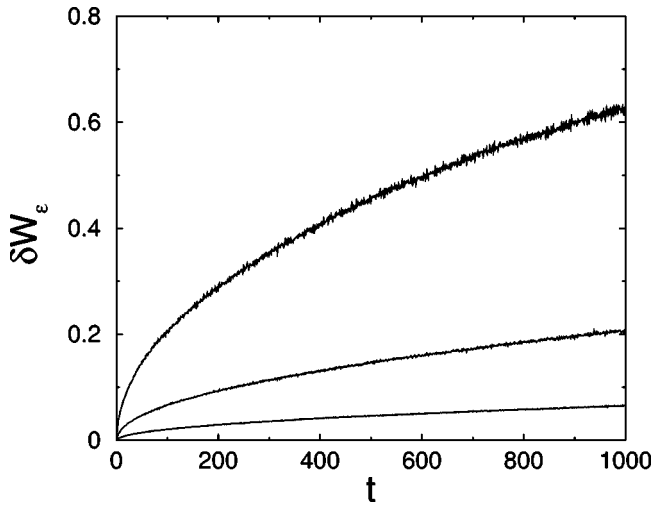

FIG. 8. Relative error on the Wigner function $\delta W_\epsilon=\langle|W-W_\epsilon|\rangle/\langle|W|\rangle$ as a function of time for $K=K_g$, $T=2\pi/N$, $N=2^{n_q}$, and $n_q=10$. The initial state is $|\Psi_0\rangle=|n_0\rangle$, with $n_0=N/2$. From bottom to top quantum noise is $\epsilon=10^{-4}$, $\epsilon=10^{-3.5}$, $\epsilon=10^{-3}$. The Wigner function is averaged over $2N$ values in the chaotic zone. Data are averaged over ten realizations of noise.

However, we should note that even if U can be implemented efficiently, $\langle\sigma^z\rangle$ can be evaluated only by iterating the procedure a number of times to get a good estimate. Therefore, the amplitude of the signal is crucial to make the whole process efficient. Thus, it is interesting to study the amplitude of peaks in the Wigner function, in order to know if strong peaks are present, which can be detected reliably through this method. This can be investigated through a quantity, which we call inverse participation ratio of the Wigner function, in analogy with the inverse participation ratio for wave functions used in quantum chaos and systems with Anderson localization [30]. For a wave function with N projections ψ_i on some basis, the inverse participation ratio $\Sigma|\psi_i|^2/(\Sigma|\psi_i|^4)$ measures the number of significant components in this basis. For the Wigner function, one has the additional sum rules $\Sigma W_i=1$ and $\Sigma W_i^2=1/N$. To define an inverse participation ratio for the Wigner function, we therefore use the formula $\xi=1/(N^2\Sigma W_i^4)$. If N peaks of approximately equal weights $1/N$ are present, then $\xi=N$, whereas N^2 components of equal weights (in absolute value) $1/N^{3/2}$ give $\xi=N^2$. Quantity ξ therefore permits to estimate the number of main components of the Wigner function. Figures 10 and 11 show the scaling of this quantity with n_q for different values of parameters. In all the cases where $T=2\pi/N$ ($N=2^{n_q}$) the ratio ξ/N^2 reaches a saturation value. This implies that asymptotically $\langle\sigma_z\rangle=NW(p,q)\sim 1/\sqrt{N}$, a value that requires N iterations followed by the measurements to be reliably estimated. In this case, the asymptotic gain in number of operations compared to the classical algorithm is only $O(\log(N))$, although the resources needed are exponentially smaller (n_q qubits instead of 2^{n_q} classical registers). This should be contrasted with the case where the number of cells increases (T constant), where Fig. 11 shows that $\xi\sim N$. This gives $\langle\sigma_z\rangle=NW(p,q)\sim 1$, which means that in this regime with localization, any of the $\sim N$ compo-

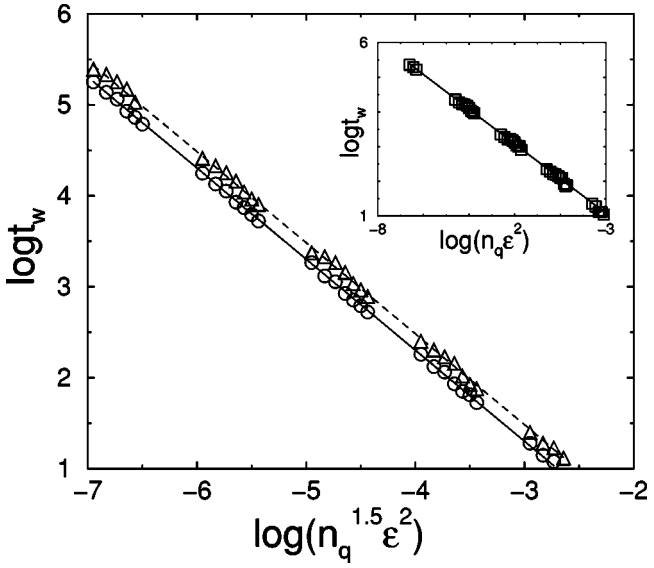

FIG. 9. Dependence of time scale t_W on system parameters for $5 \leqslant n_q \leqslant 11$. Here $K=K_g$, $T=2\pi/N$ ($N=2^{n_q}$). The Wigner function is averaged over $2N$ values in the chaotic zone ($\bigcirc$) or in the integrable zone ($\triangle$). Straight lines are theoretical formula (8) with $\alpha=1.5$ and $C_W=0.02$ (full line) or $C_W=0.03$ (dashed line). The initial state is $|\Psi_0\rangle=|n_0\rangle$, with $n_0=N/2$. Data are averaged over 10 to 1000 realizations of noise. Inset: dependence of the time scale t_W on system parameters for $5 \leqslant n_q \leqslant 14$. Here $T=0.5$ and $K=5$. The Wigner function is averaged over $2N$ values in the localized zone ($\square$). The full line is theoretical formula (8) with $\alpha=1$ and $C_W=0.012$. The initial state is $|\Psi_0\rangle=|n_0\rangle$, with $n_0=N/2$. Data are averaged over 10 to 1000 realizations of noise. Logarithms are decimal.

nents of the Wigner function which are important can be estimated reliably and efficiently through this method (provided one knows beforehand the approximate position of the localized state). The results presented in Figs. 8 and 9 show

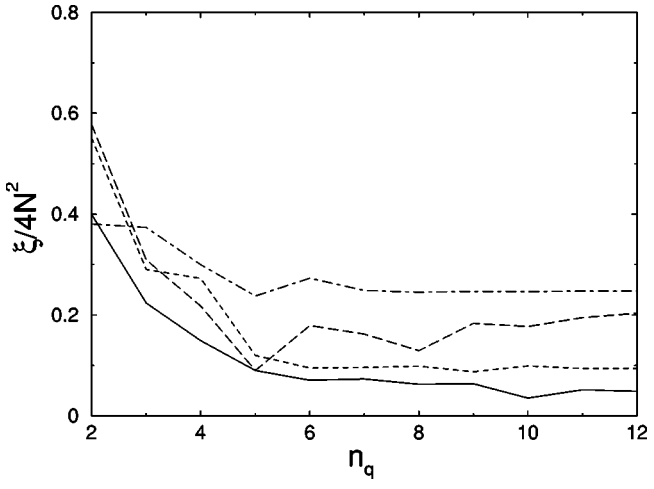

FIG. 10. Dependence of inverse participation ratio ξ of the Wigner function on the number of qubits n_q at $t=10^3$ for $T=2\pi/N$, $N=2^{n_q}$, and $K=0.5$ (full curve), $K=0.9$ (dashed curve), $K=1.3$ (long-dashed curve), $K=2.0$ (dot-dashed curve). Initial state is $|\Psi_0\rangle=|n_0\rangle$, with $n_0=1$, and $\epsilon=0$.

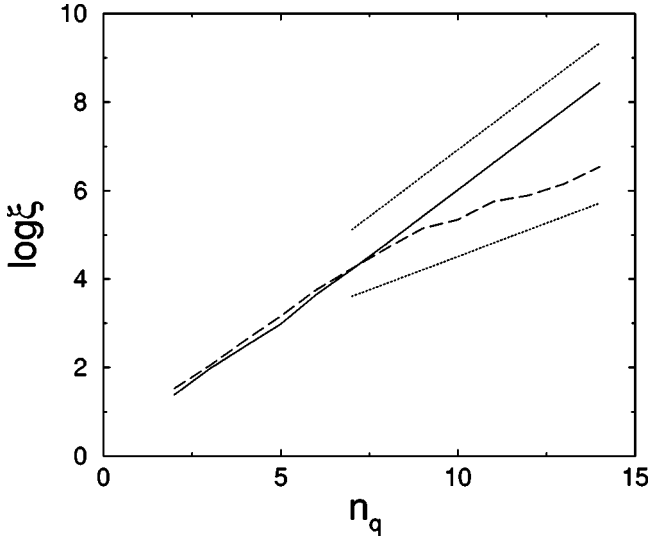

FIG. 11. Dependence of the inverse participation ratio ξ of the Wigner function on the number of qubits n_q at $t=10^3$ for $T=2\pi/N$, $N=2^{n_q}$, and $K=2$ (full line), and $T=0.5$ and $K=5$ (dashed line). Dotted lines show $\xi \propto N^2$ and $\xi \propto N$. The initial state is $|\Psi_0\rangle=|n_0\rangle$, with $n_0=1$ and $\epsilon=0$. The logarithm is decimal.

that despite the different scaling laws of $\langle|W|\rangle$, the relative errors grow only polynomially in all cases considered, thus enabling such measurements of individual values of W to be reliable for moderate amounts of noise.

V. QUANTUM TUNNELING THROUGH INVARIANT CURVES

In the preceding section, it was shown that the classical and quantum errors affect the dynamics in a rather different way. This difference is particularly striking in the régime where classical invariant curves are present (integrable or mixed systems, which correspond to moderate values of K here, as in Fig. 7). Such invariant curves cannot be crossed classically, and only quantum tunneling can transfer probability inside integrable islands from chaotic regions. Whereas small classical errors enable to cross only neighboring invariant curves, small quantum errors may lead to long-distance ''jumps'' of probability deep into integrable island (see Fig. 7, last column).

To study the effects of errors on quantum tunneling, we show in Fig. 12 the dependence of probability of the Husimi distribution $h(\theta,n)$ inside the classically forbidden region on time t. The quantity $I(t)=\int_D h(\theta,n)d\theta dn$, where D is the domain enclosed by the circle in Fig. 10 (inset), shows a linear growth with t. This can be understood by a physical argument similar to the one justifying Eq. (4). Indeed, imperfect gates transfer on average a probability of order ϵ^2 from the exact wave function to wrong phase-space positions. However, not all gates will transfer probability inside D but only a subset of them. This predicts that $I(t) \sim n_q^\alpha \epsilon^2 t$. Data from Figs. 12 and 13 and additional data (not shown) confirm this prediction, with $\alpha \approx 1.3$.

To exemplify the effect of quantum errors, Fig. 13 shows $I(t)$ at fixed time t as a function of number of qubits n_q for

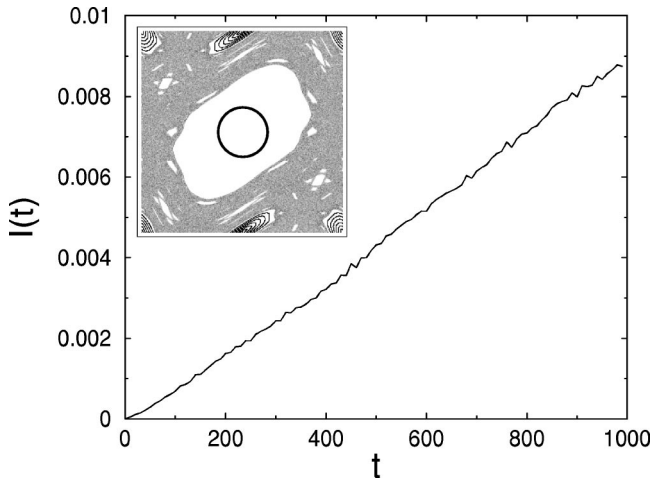

FIG. 12. Dependence of probability I of the Husimi distribution inside the circle (see text and inset) on time t for $\epsilon=10^{-3}$ and $n_q=14$ at $K=1.3$ and $T=2\pi/N$ ($N=2^{n_q}$). The initial state is $|\Psi_0\rangle=|n_0\rangle$, with $n_0=1$. Inset: The position of 100 points initially at $n_0=1$ after 10^4 iterations of classical map (1) and location of circular domain D (see text).

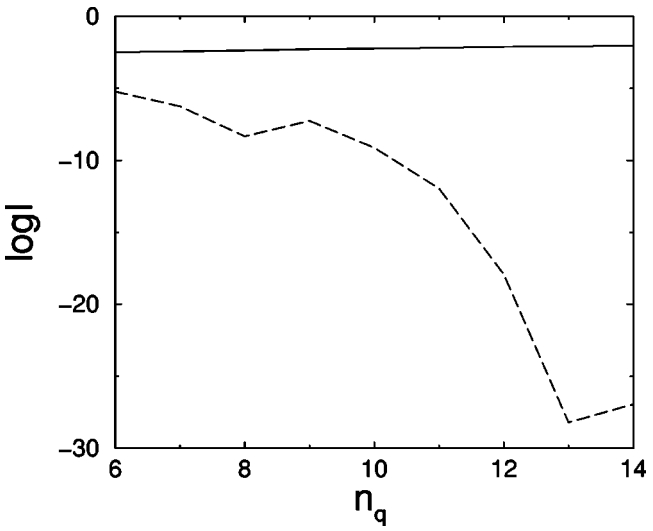

FIG. 13. Dependence of probability I of the Husimi distribution inside the circle (see text and Fig. 12) on n_q for $K=1.3$ and $T=2\pi/N$, $N=2^{n_q}$, $\epsilon=3\times10^{-3}$ (solid curve), and $\epsilon=0$ (dashed curve). Data are averaged over 100 iterations around $t=10^3$. The initial state is $|\Psi_0\rangle=|n_0\rangle$ with $n_0=1$. The logarithm is decimal.

zero and nonzero noise in the gates. In the case of zero noise, there is an exponential *decrease* with n_q. Indeed, the only process that allows to enter the island for the wave packet is quantum tunneling. In general, the probability of such a transition scales like $\exp(-S/\hbar)$, where S is a classical action. Increase of n_q amounts to decrease the effective $\hbar$ and leads to the exponential drop of I obtained numerically at $\epsilon=0$. In sharp contrast, the presence of imperfections in the gates ($\epsilon>0$) leads to direct jumps inside the island that gives an *increase* of I with n_q according to the estimate of the previous paragraph. Thus, for this specific process, the effect of noise in the gates results in a qualitative change of the dependence of tunneling probability I on n_q.

VI. CONCLUSION

The results presented in this paper show that it is possible to simulate efficiently the quantum kicked rotator on a quantum computer. For the quantum algorithm simulating the dynamics of kicked rotator, we investigated the effects of gate errors and showed that certain quantities such as fidelity and the Wigner and Husimi distributions are sufficiently robust against noise in the gates. Thus, for small amplitude of noise these quantities can be computed reliably without application of quantum error corrections. At the same time we found that there exist other characteristics, e.g., variance of probability distribution and tunneling probability inside stability islands, which are very sensitive to errors in quantum gates. In addition, the study of the Wigner function shows that individual values of this function are robust with respect to quantum errors and can be reliably estimated. However, the computation of the Wigner function at specific points meets certain readout problems in deep quasiclassical regime where generally a large number of measurements is required.

On the basis of obtained results we believe that the quantum algorithms simulating quantum chaotic maps will provide important grounds for testing the accuracy of the next generation of experimental implementations of quantum computers.

ACKNOWLEDGMENTS

We thank the IDRIS in Orsay and CalMiP in Toulouse for access to their supercomputers. This work was supported in part by the NSA and ARDA under ARO Contract No. DAAD19-01-1-0553, by the EC RTN Contract No. HPRN-CT-2000-0156, and by the project EDIQIP of the IST-FET program of the EC.

[1] R.P. Feynman, Found. Phys. **16**, 507 (1986).
[2] A. Eckert and R. Josza, Rev. Mod. Phys. **68**, 733 (1996).
[3] A. Steane, Rep. Prog. Phys. **61**, 117 (1998).
[4] M.A. Nielsen and I.L. Chuang, *Quantum Computation and Quantum Information* (Cambridge University Press, Cambridge, 2000).
[5] P.W. Shor, in *Proceedings of the 35th Annual Symposium on Foundations of Computer Science*, edited by S. Goldwasser (IEEE Computer Society, Los Alamitos, CA, 1994), p. 124.
[6] L.K. Grover, Phys. Rev. Lett. **79**, 325 (1997).
[7] L.M.K. Vandersypen, M. Steffen, G. Breyta, C.S. Yannoni, M.H. Sherwood, and I.L. Chuang, Nature (London) **414**, 883 (2001).
[8] Y.S. Weinstein, S. Lloyd, J. Emerson, and D.G. Cory, Phys. Rev. Lett. **89**, 157902 (2002).
[9] S. Lloyd, Science **273**, 1073 (1996); D.S. Abrams and S. Lloyd, Phys. Rev. Lett. **79**, 2586 (1997).
[10] A. Sørensen and K. Mølmer, Phys. Rev. Lett. **83**, 2274 (1999).

[11] R. Schack, Phys. Rev. A **57**, 1634 (1998).
[12] B. Georgeot and D.L. Shepelyansky, Phys. Rev. Lett. **86**, 2890 (2001).
[13] G. Benenti, G. Casati, S. Montangero, and D.L. Shepelyansky, Phys. Rev. Lett. **87**, 227901 (2001).
[14] B.V. Chirikov, in *Les Houches Lecture Series*, edited by M.-J. Giannoni, A. Voros, and J. Zinn-Justin (North-Holland, Amsterdam, 1991), Vol. 52.
[15] B.V. Chirikov, Phys. Rep. **52**, 263 (1979); A. Lichtenberg and M. Lieberman, *Regular and Chaotic Dynamics* (Springer, New York, 1992).
[16] P.H. Song and D.L. Shepelyansky, Phys. Rev. Lett. **86**, 2162 (2001).
[17] C. Miquel, J.P. Paz, M. Saraceno, E. Knill, R. Laflamme, and C. Negrevergne, Nature (London) **418**, 59 (2002).
[18] D.L. Shepelyansky, Physica D **28**, 103 (1987).
[19] F.M. Izrailev, Phys. Rep. **129**, 299 (1990).
[20] S. Fishman, D.R. Grempel, and R.E. Prange, Phys. Rev. Lett. **49**, 509 (1982).
[21] G. Casati, I. Guarneri, and D.L. Shepelyansky, IEEE J. Quantum Electron. **24**, 1420 (1988); P.M. Koch and K.A.H. van Leeuwen, Phys. Rep. **255**, 289 (1995).
[22] F.L. Moore, J.C. Robinson, C.F. Bharucha, B. Sundaram, and M.G. Raizen, Phys. Rev. Lett. **75**, 4598 (1995); H. Ammann, R. Gray, I. Shvarchuck, and N. Christensen, *ibid.* **80**, 4111 (1998).
[23] In Ref. [16] the noise amplitude was also $\pi\epsilon$.
[24] We note that the second moment does not grow exponentially with time at fixed n_q, but linearly. However, the coefficient of this linear growth depends exponentially on n_q.
[25] E. Wigner, Phys. Rev. **40**, 749 (1932); M.V. Berry, Philos. Trans. R. Soc. London **287**, 237 (1977).
[26] C. Miquel, J.P. Paz, and M. Saraceno, Phys. Rev. A **65**, 062309 (2002).
[27] S.-J. Chang and K.-J. Shi, Phys. Rev. A **34**, 7 (1986).
[28] T. Geisel, G. Radons, and J. Rubner, Phys. Rev. Lett. **57**, 2883 (1986); R.S. MacKay and J.D. Meiss, Phys. Rev. A **37**, 4702 (1988).
[29] W.H. Zurek, Nature (London) **412**, 712 (2001); A. Jordan and M. Srednicki, e-print quant-ph/0112139.
[30] A. MacKinnon and B. Kramer, Phys. Rev. Lett. **47**, 1546 (1981).